

Characterising the matter bispectrum of large-scale structure: halo models, perturbation theory and a three-shape model

Andrei Lazanu,^{1,*} Tommaso Giannantonio,^{2,1} Marcel Schmittfull,³ and E.P.S. Shellard¹

¹*Centre for Theoretical Cosmology, DAMTP, University of Cambridge, CB3 0WA, UK*

²*Kavli Institute for Cosmology, IoA, University of Cambridge, Madingley Road, Cambridge CB3 0HA, UK*

³*Berkeley Center for Cosmological Physics, Department of Physics and Lawrence Berkeley National Laboratory, University of California, Berkeley, California 94720, USA*

(Dated: November 9, 2015)

We study the matter bispectrum of large-scale structure by comparing the predictions of different perturbative and phenomenological models with the full three-dimensional bispectrum from N -body simulations estimated using modal methods. We show that among the perturbative approaches, effective field theory succeeds in extending the range of validity furthest on intermediate scales, at the cost of free additional parameters. By studying the halo model, we show that although it is satisfactory in the deeply non-linear regime, it predicts a deficit of power on intermediate scales, worsening at redshifts $z > 0$. By comparison with the N -body bispectrum on those scales, we show that there is a significant squeezed component underestimated in the halo model. On the basis of these results, we propose a new ‘three-shape’ model, based on the tree-level, squeezed and constant bispectrum shapes we identified in the halo model; after calibration this fits the simulations on all scales and redshifts of interest. This method provides a prototype bispectrum HALOFIT-like methodology that could be used to describe and test parameter dependencies and should be relevant for the bispectrum of weak gravitational lensing and wider applications.

Introduction — To date, power spectrum estimation has been the primary route through which to infer cosmological information from surveys of large-scale structure and the cosmic microwave sky. However, it is inevitable that the matter and galaxy bispectra (the Fourier transforms of the three-point correlators) will play an increasingly important role in the science exploitation of new data surveys. Higher-order correlators offer complementary information that breaks cosmological parameter degeneracies and probes primordial non-Gaussianity, as well as being a key diagnostic tool for nonlinear density distributions. Recently in Ref. [1] we have undertaken a comprehensive survey of perturbative and non-perturbative theoretical approaches to the matter bispectrum, presenting direct three-dimensional comparisons with the complete bispectrum obtained from N -body simulations [2]. Despite the apparent complexity of three-point correlator calculations, this work indicates that the bispectrum analysis is tractable for large-scale structure both empirically and theoretically; on the one hand, optimal and efficient modal methods can be used for bispectrum estimation and, on the other, we demonstrate that significant mathematical simplifications are available to characterise the nonlinear gravitational bispectrum. Already for the CMB, the bispectrum has become an important quantitative tool, most notably from the *Planck* satellite [3], and observational results are starting to emerge for the galaxy bispectrum, such as a recent BOSS analysis [4].

Bispectrum definitions — The statistical analysis of random fields, such as the matter density perturbation $\delta \equiv (\rho - \bar{\rho})/\bar{\rho}$, where ρ is the matter density with mean $\bar{\rho}$, involves measuring its N -point correlation functions in

real space or the equivalent polyspectra in Fourier space. We consider here the power spectrum and bispectrum,

$$\langle \delta(\mathbf{k}_1)\delta(\mathbf{k}_2) \rangle = (2\pi)^3 \delta_D(\mathbf{k}_1 + \mathbf{k}_2) P(k) \quad (1)$$

$$\langle \delta(\mathbf{k}_1)\delta(\mathbf{k}_2)\delta(\mathbf{k}_3) \rangle = (2\pi)^3 \delta_D(\mathbf{k}_1 + \mathbf{k}_2 + \mathbf{k}_3) B(k_1, k_2, k_3),$$

where δ_D is the Dirac delta function and \mathbf{k} is the wavevector with wavenumber $k_i = |\mathbf{k}_i|$. For homogeneous and isotropic primordial perturbation models, to which we restrict ourselves, the bispectrum only depends on k_1, k_2, k_3 . While the power spectrum is a function only of k , the bispectrum is a three-dimensional function defined on a tetrahedral region for which k_1, k_2, k_3 satisfy the triangle condition in Eq. (1); the gravitational bispectrum obtained from N -body simulations is plotted in Fig. 1 to illustrate this domain. In order to optimally compare two bispectra B_i and B_j in an observational context, we must define a signal-to-noise (SN) weighted scalar product between them [5]:

$$\langle B_i, B_j \rangle \equiv \frac{V}{\pi} \int_{\mathcal{V}_B} dV_k \frac{k_1 k_2 k_3 B_i(k_1, k_2, k_3) B_j(k_1, k_2, k_3)}{P(k_1)P(k_2)P(k_3)}, \quad (2)$$

where the integration domain \mathcal{V}_B is the tetrahedral region shown in Fig. 1. Using the scalar product of Eq. (2), we can define a *shape correlator* \mathcal{S} and a relative *amplitude correlator* \mathcal{A} , respectively, as

$$\begin{aligned} \mathcal{S}(B_i, B_j) &\equiv \langle B_i, B_j \rangle / \sqrt{\langle B_i, B_i \rangle \langle B_j, B_j \rangle}, \\ \mathcal{A}(B_i, B_j) &\equiv \sqrt{\langle B_i, B_i \rangle} / \sqrt{\langle B_j, B_j \rangle}. \end{aligned} \quad (3)$$

Both the amplitude and shape correlators can also be defined as binned or *sliced* quantities, by restricting the

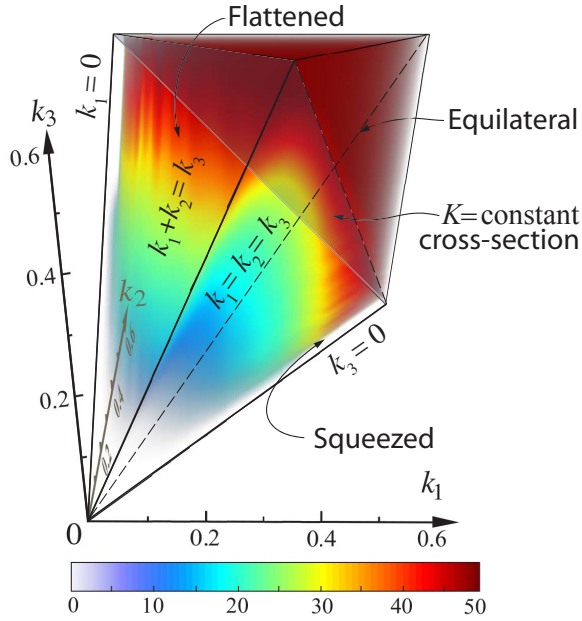


FIG. 1. The SN-weighted matter bispectrum from N -body simulations at $z=0$, showing half the tetrahedral region on which it is defined (the front half of the bispectrum has been excised to show the interior signal). The squeezed signal is located on the edges of the tetrapyd and the flattened signal on the faces, with equilateral along $k_1 = k_2 = k_3$; this diagonal line is orthogonal to the $K \equiv k_1 + k_2 + k_3 = \text{const.}$ slicing.

integration domain to narrow triangular slices at some $K \equiv k_1 + k_2 + k_3$, that is, on slices orthogonal to the tetrahedron diagonal $k_1 = k_2 = k_3$ (see Fig. 1).

As we shall see later in this letter, we can obtain an accurate global description of the non-linear gravitational bispectrum from a sum over a limited number of simple bispectrum shapes $S^i(k_1, k_2, k_3)$, provided that we have the flexibility to calibrate an overall scale-dependent amplitude $f(K)$. The constant shape is simply given by

$$S^{\text{const}}(k_1, k_2, k_3) = 1 \text{ (Mpc}/h)^6. \quad (4)$$

The second shape is ‘squeezed’ and can be expressed in terms of the linear power spectrum $P(k)$ as

$$S^{\text{squeez}}(k_1, k_2, k_3) = \frac{1}{3} [P(k_1)P(k_2) + P(k_2)P(k_3) + P(k_3)P(k_1)] . \quad (5)$$

The third shape is the leading-order bispectrum of LSS:

$$S^{\text{tree}}(k_1, k_2, k_3) = 2P(k_1)P(k_2)F_2^{(s)}(\mathbf{k}_1, \mathbf{k}_2) + 2P(k_2)P(k_3)F_2^{(s)}(\mathbf{k}_2, \mathbf{k}_3) + 2P(k_3)P(k_1)F_2^{(s)}(\mathbf{k}_3, \mathbf{k}_1), \quad (6)$$

where the standard gravitational kernel $F_2^{(s)}$ is discussed in Ref. [1]. The actual bispectrum is more closely approximated by the tree-level shape (Eq. 6) if we replace P by the nonlinear HALOFIT [6, 7] P_{NL} power spectrum

[8]; we denote the improved shape by S^{treeNL} . Putting this all together we obtain the ‘three-shape’ model [1]:

$$B_{3\text{-shape}}(k_1, k_2, k_3) = f_{1h}(K) S^{\text{const}}(k_1, k_2, k_3) + f_{2h}(K) S^{\text{squeez}}(k_1, k_2, k_3) + f_{3h}(K) S^{\text{treeNL}}(k_1, k_2, k_3). \quad (7)$$

Perturbation theory — Perturbative approaches expand the density contrast δ in a series of perturbations $\delta^{(n)}$, which are valid while $|\delta| \ll 1$ [9]; this is true at early times and on large scales. In Eulerian standard perturbation theory (SPT), expansions in terms of powers of the variable δ are considered. The leading-order tree-level bispectrum labelled B_{211} is given by Eq. (6) [10]. For the one-loop correction in SPT, four additional terms are added to this, labelled B_{222} , $B_{321}^{(I)}$, $B_{321}^{(II)}$ and B_{411} [9]. These terms only succeed in extending the range of validity of the tree-level (Eq. 6) by a small amount and yield an excess of power on quasi-nonlinear scales (essentially because loop integrals require integration of momenta over an infinite range where the $|\delta| \ll 1$ assumption is no longer valid).

The observation that even when the density fluctuations are no longer small the gravitational potential still remains small, together with this excess, has led to the development of the effective field theory of LSS (EFT) [11, 12]. In this theory there are additional parameters that quantify the effects of non-perturbative small-scale physics on large scales through an effective stress-energy tensor. The power spectrum and bispectrum are modified at leading order by adding terms to each of them [13, 14], which include parameters calibrated on simulations. However, the leading EFT bispectrum counter-term is calibrated using only the power spectrum.

Another method that improves the accuracy of the prediction is renormalised perturbation theory (RPT) [15]; the SPT expansion is reorganised and then resummed. The calculations simplify significantly with the MPT-BREEZE method [16], which expresses power spectrum and bispectrum directly in terms of the positive-definite SPT terms, but multiplied by a decaying exponential function. Alternatively, Lagrangian perturbation theory displaces particles from their Lagrangian initial positions [17]. By considering the expansion of the mass density in these displacements and using a suitable resummation, the resummed Lagrangian perturbation theory (RLPT) is obtained [18, 19].

In Ref. [1] we survey all the above-mentioned methods and calculate the bispectrum (even up to some two-loop terms). By considering the sliced shape correlators \mathcal{S} of each theory bispectrum with the three canonical shapes (Eqs. 4-6), we show all the perturbative approaches can be well approximated by the ‘flattened’ tree-level shape (6) (see Fig. 6 in Ref. [1]).

Phenomenological models — The halo model extends the modelling of dark matter clustering into the nonlinear regime, by assuming that all dark matter in the Universe

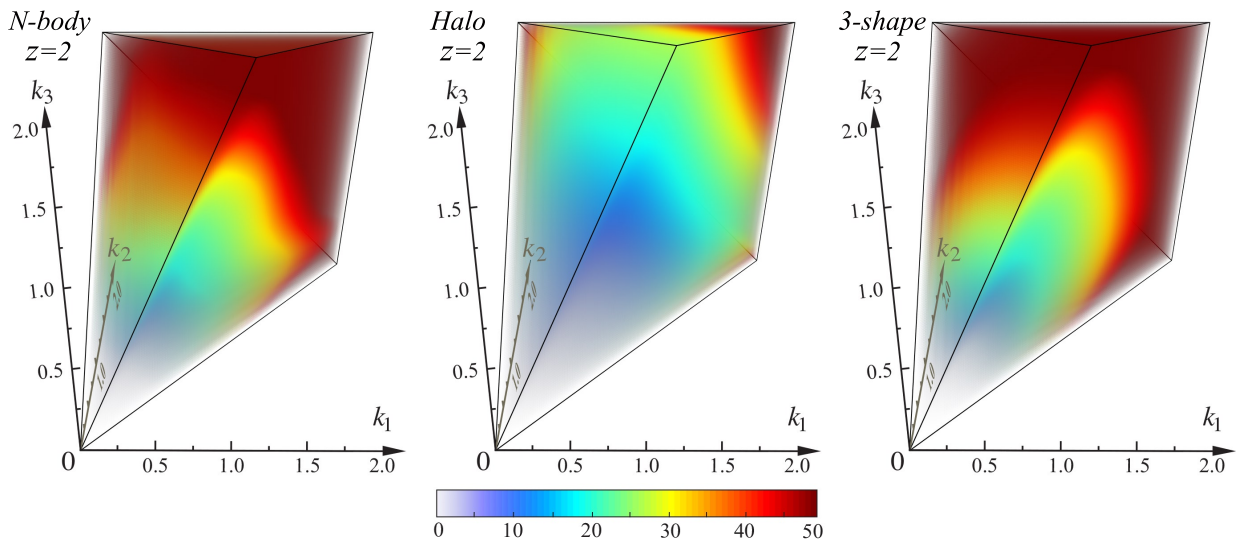


FIG. 2. The SN-weighted matter bispectrum at $z=2$: we compare the N -body bispectrum (left) with the standard halo model (middle) and the ‘three-shape’ model (right). The halo model for $z > 0$ exhibits a large deficit (including a missing squeezed component), while the ‘three-shape’ model shows improved agreement with the N -body results.

has collapsed into haloes [20]. The halo model power spectrum and bispectrum are composed of two and three terms respectively, corresponding to pairs or triplets of particles residing in one, two, or three haloes. The three bispectrum components are labelled B_{1h} , B_{2h} and B_{3h} , and they contribute mainly to the fully nonlinear regime, to intermediate scales and perturbative limit respectively.

The halo model provides a satisfactory description of N -body simulations at $z=0$ in the fully nonlinear regime, but it has some well-known shortcomings even at late times [20, 21]: (a) in the transition between the linear and non-linear regimes, the accuracy of the model is at the sub-10% level; (b) on very large scales P_{1h} , B_{1h} and B_{2h} do not decay to zero, thus leading to an excess of power with respect to linear theory; and (c) the assumption that all matter in the Universe has collapsed into haloes at all redshifts leads to growing inaccuracies for $z > 0$.

The first two problems can be improved by combining the halo model with perturbation theory [22], which we call the ‘halo-PT model’. This cuts off excess power in the 1- and 2-halo terms with a prescription that endeavours to ensure three particles contribute to only one of the terms. This modifies B_{1h} and B_{2h} , while B_{3h} is substituted with the perturbative prediction, for which we use EFT in our implementation [1].

By analysing the bispectrum shapes of the three halo model components, we find that the 1-, 2- and 3-halo terms have excellent sliced shape correlations \mathcal{S} (Eq. 3) with the constant (Eq. 4), squeezed (Eq. 5) and tree-level (Eq. 6) shapes respectively, for all redshifts considered (see Fig. 7 of Ref. [1]). This provided a key motivation for proposing the three-shape model defined in Eq. (7).

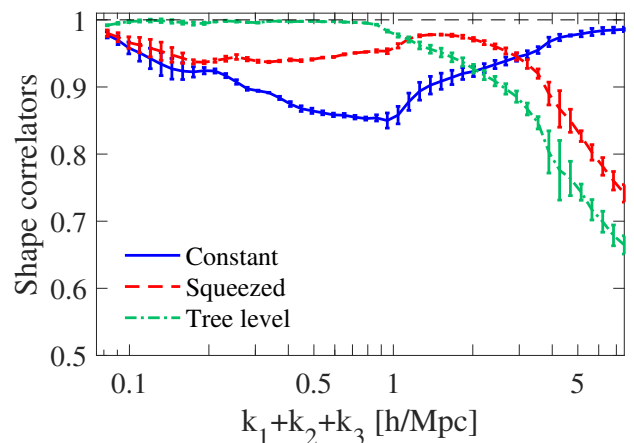


FIG. 3. Sliced shape correlations between the N -body bispectrum and the three canonical shapes (Eqs. 4-6) at $z=1$. A linear combination offers good shape correlations at all k .

Simulations and benchmark model — To calculate the matter bispectrum we analyse density distributions from three sets of N -body simulations with Gaussian initial conditions described in Ref. [2]. The signal-to-noise weighted bispectrum \hat{B} is reconstructed using a separable modal basis Q_n [5] as

$$\frac{B(k_1, k_2, k_3) \sqrt{k_1 k_2 k_3}}{\sqrt{P(k_1)P(k_2)P(k_3)}} = \sum_{n=0}^{n_{\max}} \beta_n^Q Q_n(k_1, k_2, k_3), \quad (8)$$

where about 100 β_n^Q coefficients were required for good convergence. The three simulations cover k -ranges $[0.0039, 0.5] h/\text{Mpc}$, $[0.016, 2.0] h/\text{Mpc}$ and

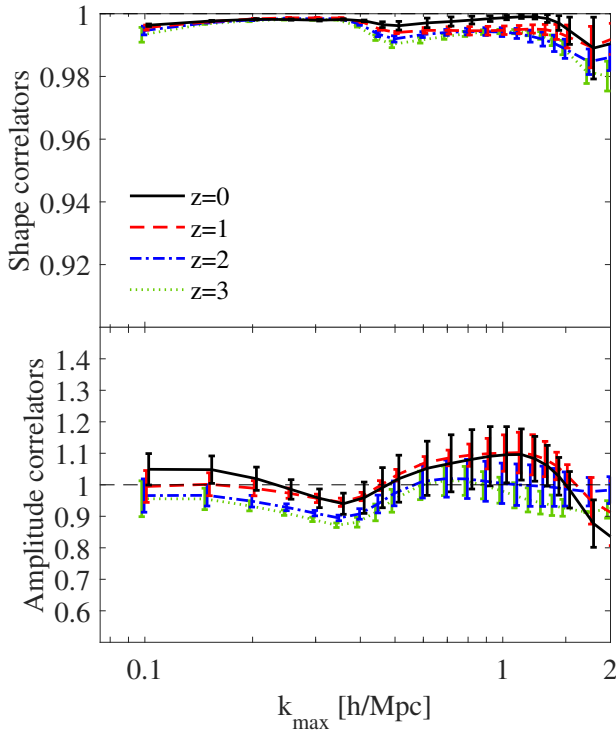


FIG. 4. Shape (upper) and amplitude (lower) correlators between the measured N -body matter bispectrum and the ‘three-shape’ model at four redshifts. The correlators are defined with Eq. (2) integrated up to the wavenumber k_{\max} .

$[0.062, 8.0] h/\text{Mpc}$ respectively and are combined with a smoothing function, explained in Ref. [1]. Plots of the full 3D SN-weighted bispectrum obtained at $z = 0, 2$ in Figs. 1 and 2 (left) show qualitatively how shape changes with scale and redshift. A quantitative analysis of the N -body bispectrum using the sliced shape correlator (Eq. 3) is summarised in Fig. 3. The flattened tree-level shape (Eq. 6) is an excellent approximation at small wavenumbers k , while the constant shape (Eq. 4) dominates for large k on nonlinear scales. On intermediate scales, an additional squeezed component (Eq. 5) prevails. In combination, these results confirm the proposed ‘three-shape’ model (Eq. 7), which we describe in more detail in Ref. [1], together with the numerical values of the parameters used to calibrate simple forms of $f_{1h}(K)$, $f_{2h}(K)$ and $f_{3h}(K)$.

On large scales the three-shape model is based on the non-linear tree-level bispectrum (or any perturbative approach, e.g. EFT), but this leads to an excessive amplitude on intermediate scales. To alleviate this problem requires a prescription to prevent double-counting in f_{3h} , so we introduce an exponential cut-off which adds one free parameter. On small scales, the one-loop bispectrum provides an adequate description, so we use a simple fit f_{1h} to this, accurate at all redshifts and introducing

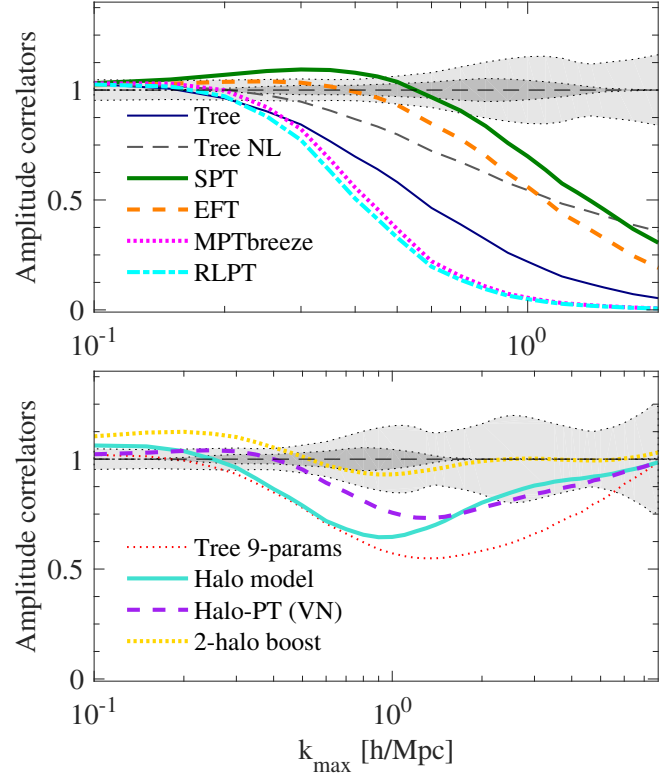


FIG. 5. Amplitude correlators at $z = 1$ between the benchmark ‘three-shape’ model and all perturbative approaches (upper) and halo models (lower). Shape correlators are higher.

no extra parameters. In the intermediate regime corresponding to the two-halo term, the standard halo model shows a power deficit that worsens at higher redshift (see Fig. 2, middle panel). We find that the two-halo deficit can be reduced by boosting this term by approximately $D(z)^{-1.7}$, where $D(z)$ is the linear growth factor normalised to unity today. However, this is not entirely satisfactory, because it increases the excess on small scales as $k \rightarrow 0$. To improve the accuracy of this term, we model f_{2h} with a simple function, scaling as $f_{2h} \propto K^3$ for $K \rightarrow 0$. We fix the functional form and introduce two free parameters calibrated to simulations. We show in Fig. 4 that the ‘three-shape’ model thus obtained fits the simulations well for all wavenumbers k and redshifts z considered (shape correlation $\mathcal{S} > 98\%$ and relative amplitude $\mathcal{A} \simeq 1$ within 10%).

Testing theoretical approaches — We next use the calibrated ‘three-shape’ model (Eq. 7) as a reference benchmark against which to test the accuracy of other perturbative and halo models using the amplitude \mathcal{A} and shape correlators \mathcal{S} . The results at $z = 1$ are shown in Fig. 5 with light and dark grey areas representing, respectively, uncertainties between simulation realisations

and the inaccuracy in $B_{3\text{-shape}}$ (see Ref. [1] for further details). For the perturbative theories in Fig. 5 (upper panel), we see the generic result that SPT produces an excess on mildly nonlinear scales before starting to decay in the nonlinear regime. This excess is removed in EFT by adding a counterterm calibrated to simulations, thus offering reasonable accuracy over an extended k -range. RPT (MPTBREEZE) and RLPT produce accurate results on very large scales (small k), with the accuracy increasing as the number of loops is increased (we also calculated the two-loop bispectrum in the MPTBREEZE formalism for a few slices). Both methods cut off the excess seen in SPT with physically-motivated exponential functions, which causes the sharp decay beyond the linear regime. Of all these methods, we conclude that EFT succeeds in extending the validity range furthest into the nonlinear regime. However, the much simpler nonlinear tree-level approximation ('treeNL') also provides a useful extrapolation for the bispectrum at higher k . More quantitatively, we find that at $z = 1$ SPT is accurate at the 5% level up to $k = 0.14 h/\text{Mpc}$; EFT extends this to $k = 0.36 h/\text{Mpc}$, while MPTBREEZE and RLPT are limited to $k = 0.21 h/\text{Mpc}$, $k = 0.19 h/\text{Mpc}$ respectively, comparable with the treeNL approach ($k = 0.22 h/\text{Mpc}$).

Although the standard halo model provides an adequate fit for the bispectrum at $z = 0$, at higher redshifts a significant deficit appears on intermediate scales, as shown at $z = 1$ in Fig. 5 (lower panel). For $z \geq 2$, this deficit becomes larger than a factor of 2, reflecting the incorrect underlying growth rate of the two-halo term, a problem shared by the halo-PT model which is also plotted. Boosting the two-halo signal at higher redshift can alleviate the intermediate deficit, but it creates an excess at small k . The standard halo model clearly requires a substantially modified two-halo term, combined with an improved perturbative approximation (such as the nonlinear tree-level or the EFT models), any of which can be easily incorporated into the three-shape model.

Conclusion — In this letter we have weighed the relative merits of a broad range of theoretical bispectrum models through a quantitative comparison with the full 3D matter bispectrum estimated from N -body simulations. Inspired by the three canonical shapes we identified in the halo model, we have developed a simple phenomenological three-shape model which can achieve a good match to the N -body bispectrum for all redshifts $z < 3$. In future, we will improve the precision of the three-shape model by calibrating it on higher-resolution simulations: this will be useful to test parameter dependencies and eventually to provide a HALOFIT-like bispectrum model, with applications e.g. to weak gravitational

lensing. We will extend this modelling to the bispectrum of biased tracers, as well as primordial non-Gaussianity.

Acknowledgements — This work used the COSMOS SMP supercomputer at DAMTP, Cambridge, operated on behalf of the STFC DiRAC HPC Facility, and it was supported by STFC grants ST/J005673/1, ST/H008586/1, ST/K00333X/1 and STM007065/1.

* A.Lazanu@damtp.cam.ac.uk

- [1] A. Lazanu, T. Giannantonio, M. Schmittfull, and E. P. S. Shellard, (2015), arXiv:1510.04075 [astro-ph.CO].
- [2] M. M. Schmittfull, D. M. Regan, and E. P. S. Shellard, Phys. Rev. D **88**, 063512 (2013).
- [3] Planck Collaboration, ArXiv e-prints (2015), arXiv:1502.01582.
- [4] H. Gil-Marín, J. Noreña, L. Verde, W. J. Percival, C. Wagner, M. Manera, and D. P. Schneider, Mon. Not. R. Astron. Soc. **451**, 5058 (2015).
- [5] J. R. Fergusson, D. M. Regan, and E. P. S. Shellard, Phys. Rev. D **86**, 063511 (2012).
- [6] R. E. Smith, J. A. Peacock, A. Jenkins, S. D. M. White, C. S. Frenk, F. R. Pearce, P. A. Thomas, G. Efstathiou, and H. M. P. Couchman, Mon. Not. R. Astron. Soc. **341**, 1311 (2003).
- [7] R. Takahashi, M. Sato, T. Nishimichi, A. Taruya, and M. Oguri, Astrophys. J. **761**, 152 (2012).
- [8] R. Scoccimarro and H. M. P. Couchman, Mon. Not. R. Astron. Soc. **325**, 1312 (2001).
- [9] F. Bernardeau, S. Colombi, E. Gaztañaga, and R. Scoccimarro, Physics Reports **367**, 1 (2002).
- [10] J. N. Fry, Astrophys. J. **279**, 499 (1984).
- [11] D. Baumann, A. Nicolis, L. Senatore, and M. Zaldarriaga, J. Cosmol. Astropart. Phys. **2012**, 051 (2012).
- [12] J. Carrasco, M. Hertzberg, and L. Senatore, Journal of High Energy Physics **2012**, 82 (2012).
- [13] R. E. Angulo, S. Foreman, M. Schmittfull, and L. Senatore, (2014), arXiv:1406.4143 [astro-ph.CO].
- [14] T. Baldauf, L. Mercolli, M. Mirbabayi, and E. Pajer, J. Cosmol. Astropart. Phys. **5**, 007 (2015).
- [15] M. Crocce and R. Scoccimarro, Phys. Rev. D **73**, 063519 (2006).
- [16] M. Crocce, R. Scoccimarro, and F. Bernardeau, Mon. Not. R. Astron. Soc. **427**, 2537 (2012).
- [17] J. Ehlers and T. Buchert, General Relativity and Gravitation **29**, 733 (1997).
- [18] T. Matsubara, Phys. Rev. D **77**, 063530 (2008).
- [19] C. Rampf and T. Buchert, J. Cosmol. Astropart. Phys. **6**, 021 (2012), arXiv:1203.4260 [astro-ph.CO].
- [20] A. Cooray and R. Sheth, Physics Reports **372**, 1 (2002).
- [21] R. E. Smith, R. K. Sheth, and R. Scoccimarro, Phys. Rev. D **78**, 023523 (2008).
- [22] Valageas, P. and Nishimichi, T., A&A **532**, A4 (2011).